Three-dimensional reconstructions of the putative metazoan *Namapoikia* show that it was a microbial construction

Akshay Mehra[a,b,c,1], Wesley A. Watters[d], John P. Grotzinger[e], and Adam C. Maloof[a]

[a]Department of Geosciences, Princeton University, Princeton, NJ 08544; [b]Neukom Institute, Dartmouth College, Hanover, NH 03755; [c]Department of Earth Sciences, Dartmouth College, Hanover, NH 03755; [d]Department of Astronomy, Wellesley College, Wellesley, MA 02481; and [e]Division of Geological and Planetary Sciences, California Institute of Technology, Pasadena, CA 91125

Edited by Andrew H. Knoll, Harvard University, Cambridge, MA, and approved June 23, 2020 (received for review May 12, 2020)

Strata from the Ediacaran Period (635 million to 538 million years ago [Ma]) contain several examples of enigmatic, putative shell-building metazoan fossils. These fossils may provide insight into the evolution and environmental impact of biomineralization on Earth, especially if their biological affinities and modern analogs can be identified. Recently, apparent morphological similarities with extant coralline demosponges have been used to assign a poriferan affinity to *Namapoikia rietoogensis*, a modular encrusting construction that is found growing between (and on) microbial buildups in Namibia. Here, we present three-dimensional reconstructions of *Namapoikia* that we use to assess the organism's proposed affinity. Our morphological analyses, which comprise quantitative measurements of thickness, spacing, and connectivity, reveal that *Namapoikia* produced approximately millimeter-thick meandering and branching/merging sheets. We evaluate this reconstructed morphology in the context of poriferan biology and determine that *Namapoikia* likely is not a sponge-grade organism.

3D reconstruction | Ediacaran | early life

In the Late Ediacaran (~550 Ma), microbe-dominated reefs bore witness to the arrival of putative biomineralizing metazoans. By the Cambrian radiation [beginning 538.6 Ma to 538.8 Ma (1)], a time period during which most modern animal phyla first emerged, skeletal reef dwellers were producing framework constructions and effectively engineering their surroundings (2). Today, biomineralizing organisms are responsible for building some of Earth's largest organic constructions (e.g., the Great Barrier Reef), which is indicative of the outsize impact that biomineralization has had on the planet's sedimentological, biological, and geochemical makeup.

To understand when, where, and why animals began to biomineralize, as well as to determine the environmental, ecological, and evolutionary ramifications associated with the first biomineralizers, it is necessary to study the earliest skeletal metazoan fossil record. This record comprises four genera from Ediacaran shallow water settings: *Namacalathus*, *Cloudina*, *Sinotubulites*, and *Namapoikia* (3). Although morphologically simple, these organisms have proven to be enigmatic, and their growth habits, biological affinities, and environmental impacts are the subject of ongoing debate.

With respect to early biomineralization, modes of shell building appear to have varied among the Ediacaran putative biomineralizers. Exactly how, and to what degree, each organism made hard parts remains unresolved. Workers have suggested that *Namacalathus*, a flexible, goblet-shaped organism, produced a foliated calcitic ultrastructure (4). Conversely, *Namacalathus* also has been shown to have been lightly calcified (5, 6). *Cloudina*, a tubular organism made up of a "cup in cup" morphology, was thought to have precipitated carbonate on an organic matrix (5, 7). More recent work, however, has demonstrated that phosphatized *Cloudina* share a nanoparticulate fabric with extant biomineralizers, suggesting that the organism formed skeletons in the same way as modern animals (8). That said, reconstructions of *Cloudina*, made to test the assertion that the organism built wave-resistant frameworks (9, 10), revealed that aggregates comprise transported and deformed individuals (11), furthering the idea that *Cloudina* produced weakly-to-non-biomineralized tubes. *Sinotubulites*, another tubular organism, also had plastic walls, but ones that were made up of a predominately organic matrix (12).

Recently, researchers have proposed that *Namapoikia*, a labyrinthine encrusting construction, produced skeletal material by rapidly calcifying an organic scaffold (13). Studies of polished, two-dimensional (2D) transverse and longitudinal sections of *Namapoikia* suggest a complex interplay between the construction and surrounding microbial growths, with the two life forms competing and, in some cases, repeatedly encrusting over one another (13). Workers have proposed that *Namapoikia* shares morphological characteristics with Chaetetid sponges and have inferred a biomineralizing pathway that is like that of the extant demosponges *Vaceletia* and *Acanthochaetetes* (13, 14). On the basis of these similarities, *Namapoikia* has been assigned a poriferan affinity.

Molecular clock and phylogenetic estimates (15) suggest that poriferans evolved during the Cryogenian Period (720 Ma to 635 Ma). Indeed, the Precambrian fossil record is replete with examples of purported sponge remains. Spicules, biomarkers, and even full body fossils, all older than the onset of the Ediacaran Period, have been described—and debated—by researchers (for a complete review, see ref. 16; also see refs. 17 and 18 for more recent examples of debate). Additionally, by the early Cambrian,

Significance

Animals that build skeletons have an outsized impact on Earth's biological, geochemical, and sedimentological cycles. To determine when, where, and why metazoan biomineralization first emerged, it is necessary to study the earliest record of skeletal animals. This record is made up of four genera from the Ediacaran period: *Namacalathus*, *Cloudina*, *Sinotubulites*, and *Namapoikia*. Here, we measure three-dimensional reconstructions of *Namapoikia* to test the hypothesis that it is a calcifying sponge. We find that *Namapoikia* lacks the physical characteristics expected of a sponge, or, for that matter, an animal.

Author contributions: A.M., W.A.W., J.P.G., and A.C.M. designed research; A.M. performed research; A.M. and A.C.M. analyzed data; and A.M. and A.C.M. wrote the paper.

The authors declare no competing interest.

This article is a PNAS Direct Submission.

Data deposition: The computational source code used in this paper is available in GitHub at https://github.com/giriprinceton/namapoikia.

See online for related content such as Commentaries.

[1]To whom correspondence may be addressed. Email: akmehra@alumni.princeton.edu.

This article contains supporting information online at https://www.pnas.org/lookup/suppl/doi:10.1073/pnas.2009129117/-/DCSupplemental.

First published August 3, 2020.

calcifying organisms of definitive poriferan affinity were present on Earth, and some sponges, namely the Archaeocyathids, were even responsible for the world's first framework reefs (2). It stands to reason that poriferans, having appeared during the Cryogenian and eventually becoming the dominant engineers of the Early Cambrian, may have first evolved the ability to build calcified skeletons during the Late Ediacaran. To test this idea, we seek to determine whether *Namapoikia* is, in fact, a sponge-grade organism.

Like many other Ediacaran fossils, specimens of *Namapoikia* lack soft tissue preservation and exhibit signs of diagenetic alteration (e.g., recrystallization). As a result, it is necessary to analyze the gross morphological characteristics of *Namapoikia* specimens, such as the size, shape, and distribution of structures, in order to describe growth habit, identify possible analogs, and evaluate biological affinity. Since 2D measurements (e.g., made on polished slabs or on bedding planes in outcrop) are subject to misinterpretation and measurement error (11), three-dimensional (3D) data are required for accurate analysis. Unfortunately, *Namapoikia* skeletons are preserved as carbonate minerals within carbonate rock, precluding isolation via acid dissolution or imaging with traditional, density-sensitive techniques. To address this problem, we utilize serial grinding and imaging, a method which relies on color and texture to differentiate between features of interest (e.g., fossils) and the surrounding matrix (6, 11, 19). The resulting 3D reconstructions, combined with field observations, enable us to quantitatively assess the affinity and paleoecology of *Namapoikia*.

Geologic Setting, Field Observations, and Reconstructions

In situ examples of *Namapoikia* are found in a pinnacle reef outcropping on Driedoornvlakte Farm near Reitoog, Namibia (WGS84 UTM 33K 667792E 7358951N; Fig. 1 *A* and *B*). These rocks are part of the Kuibis Subgroup (Omkyk Member) of the Neoproterozoic Nama Group. They formed on a carbonate ramp in the northern Zaris subbasin coincident with convergence along the Damara and Gariep orogens (20, 21). There are no direct radiometric dates from the Driedoornvlakte stratigraphy. However, uranium–lead zircon ages from the Kuibis constrain the maximum depositional age to 548.8 ± 1 Ma (20). Additionally, a uranium–lead zircon date in the overlying Schwarzrand subgroup (22) provides a minimum deposition age of 545.41 ± 1 Ma.

The reef at Driedoornvlakte Farm, which is 500 m thick, 10 km long, and dips 25 to 40° to the southeast, sits on Precambrian quartzite. The carbonate ramp was created over the course of three distinct accommodation cycles; in the final stage, just prior to drowning by shales of the Urikos Member, pinnacle buildups developed on the platform margins (21). These pinnacles comprise microbial mounds made up of a combination of columnar or encrusting stromatolites and columnar or massive thrombolites. Both *Cloudina* and *Namacalathus* can be found in the fill between microbial buildups and in clinoformal grainstones. *Namapoikia* is found encrusting the walls and tops of microbial buildups in decimeter-wide neptunian dykes (Fig. 1 *D* and *E*), which are shallow fractures in the reef that opened to the seafloor.

Individual *Namapoikia* can be up to 1 m wide and up to 0.25 m tall (13, 23). *Namapoikia* specimens comprise regularly spaced, millimeter-thick structural elements, here referred to as "partitions." These elements split and merge in transverse and longitudinal directions (see Fig. 2 for a visual reference to the spatial conventions used in this work). In certain specimens, partitions have been said to be intersected by perpendicular tabulae (13). A detailed survey of the pinnacle reef at Driedoornvlakte reveals that *Namapoikia* is rare, occurring in 3% of observed locations (Fig. 1*C*). To the best of our knowledge, *Namapoikia* has not been described in other, contemporaneous rocks in Namibia or, for that matter, anywhere else on Earth.

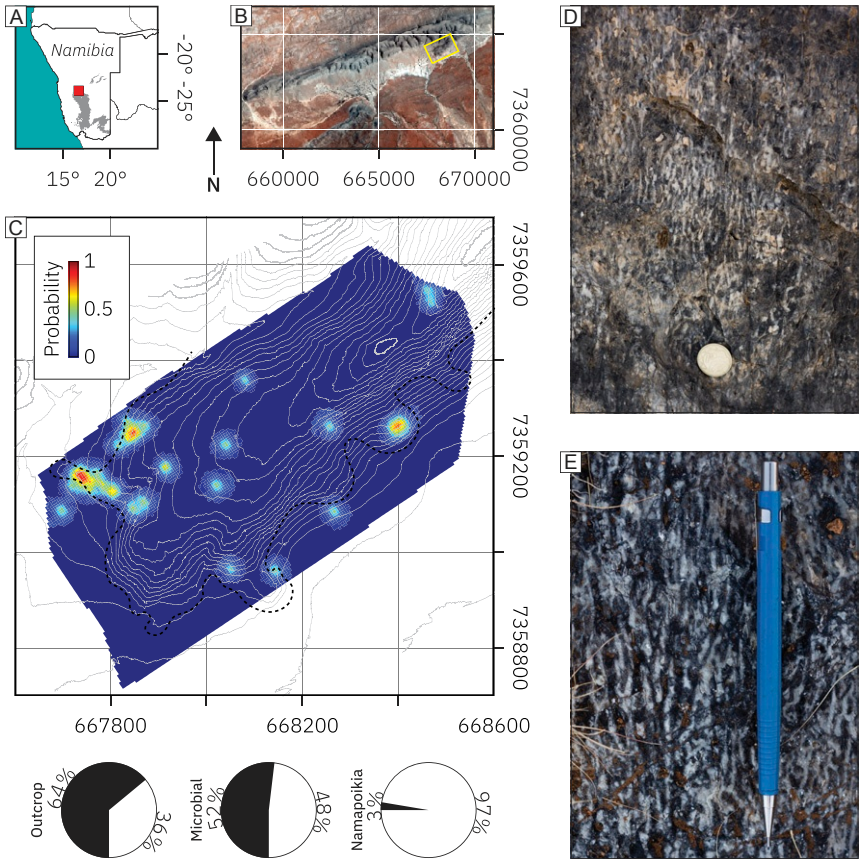

Fig. 1. Field observations. (*A*) Location of the study area in Namibia. The red square is Driedoornvlakte Farm, while the light gray fill depicts the geographic extent of Nama Group rocks. (*B*) View of the reef complex at Driedoornvlakte Farm, with the study area marked by the yellow rectangle. (*C*) (*Top*) Interpolated survey data showing the occurrence of *Namapoikia* in the reef. The contour interval is 5 m; contours were generated from a drone imagery-derived digital surface model (11). (*Bottom*) Pie charts depicting the percent of observed locations exhibiting a feature (presence of feature denoted in black). (*D* and *E*) Field photographs of in situ *Namapoikia*. Map coordinates in *B* and *C* are with reference to WGS84 UTM 33K.

We reconstruct and measure two specimens of *Namapoikia* (referred to as sample A and sample B) from the pinnacles at Driedoornvlakte Farm. Both samples comprise white, calcified partitions surrounded by a matrix of fine-grained, black micrite fill (Fig. 2 *A* and *B*). The fill contains no evident syndepositional sedimentary structures. Blocky calcite spar occurs throughout both samples and appears to replace fill between the partitions (Fig. 2 *A* and *B*). Sample A includes a small amount of yellow dolomite (approximately 1.6% by volume, occurring predominately along fracture planes). Sample B is bounded by microbial textures (Fig. 2*B*). A petrographic thin section of sample A reveals that the fossil and matrix phases are recrystallized.

When reconstructed, partitions meander, branch, and merge in transverse and longitudinal sections with no evidence of tabulae (Fig. 2 *C* and *D*) (*SI Appendix*, Fig. S1*F* and Movies S1 and S2). Partition thickness and spacing vary between the two samples. In sample A, partitions have a thickness of 640/1,030/1,393 μm (25th/50th/75th percentiles; this convention is used through the remainder of the text), while the interpartition voids have a thickness of 1,559/2,402/3,547 μm (Fig. 3*B*). In sample B, partitions have a thickness of 539/831/1,122 μm, and the interpartition voids have a thickness of 735/1,221/1,881 μm. A two-sample Kolmogorov–Smirnov test of partition thicknesses rejects the null hypotheses that the populations are from a single distribution ($P < 0.001$, $D = 0.19$; D refers to the magnitude of the Kolmogorov–Smirnov statistic). The same test on interpartition thicknesses also rejects the null hypothesis ($P < 0.001$, $D = 0.41$).

Notably, both samples A and B contain large, irregularly distributed voids. To test whether the presence of these voids contributes to the differences in partition and interpartition thicknesses between the two samples, representative subvolumes—comprising regularly spaced partitions and referred to as subvolume A and subvolume B—are chosen and measured (Fig. 3*D*). Within these selected regions, disparities between the two samples persist. In subvolume A, partitions have a thickness of 430/856/1,204 μm, and interpartition voids have a thickness of 1,285/1,811/2,377 μm, while, in subvolume B, partitions have a thickness of 566/781/1,020 μm, and interpartition voids have a thickness of 671/1,005/1,435. A two-sample Kolmogorov–Smirnov test of partition thicknesses rejects the null hypothesis that the populations are from the same distribution ($P < 0.001$, $D = 0.14$), as does a test of interpartition thicknesses ($P < 0.001$, $D = 0.44$).

The median thickness of partitions varies with respect to height in each sample (Fig. 3*E*). When applying a best-fit line

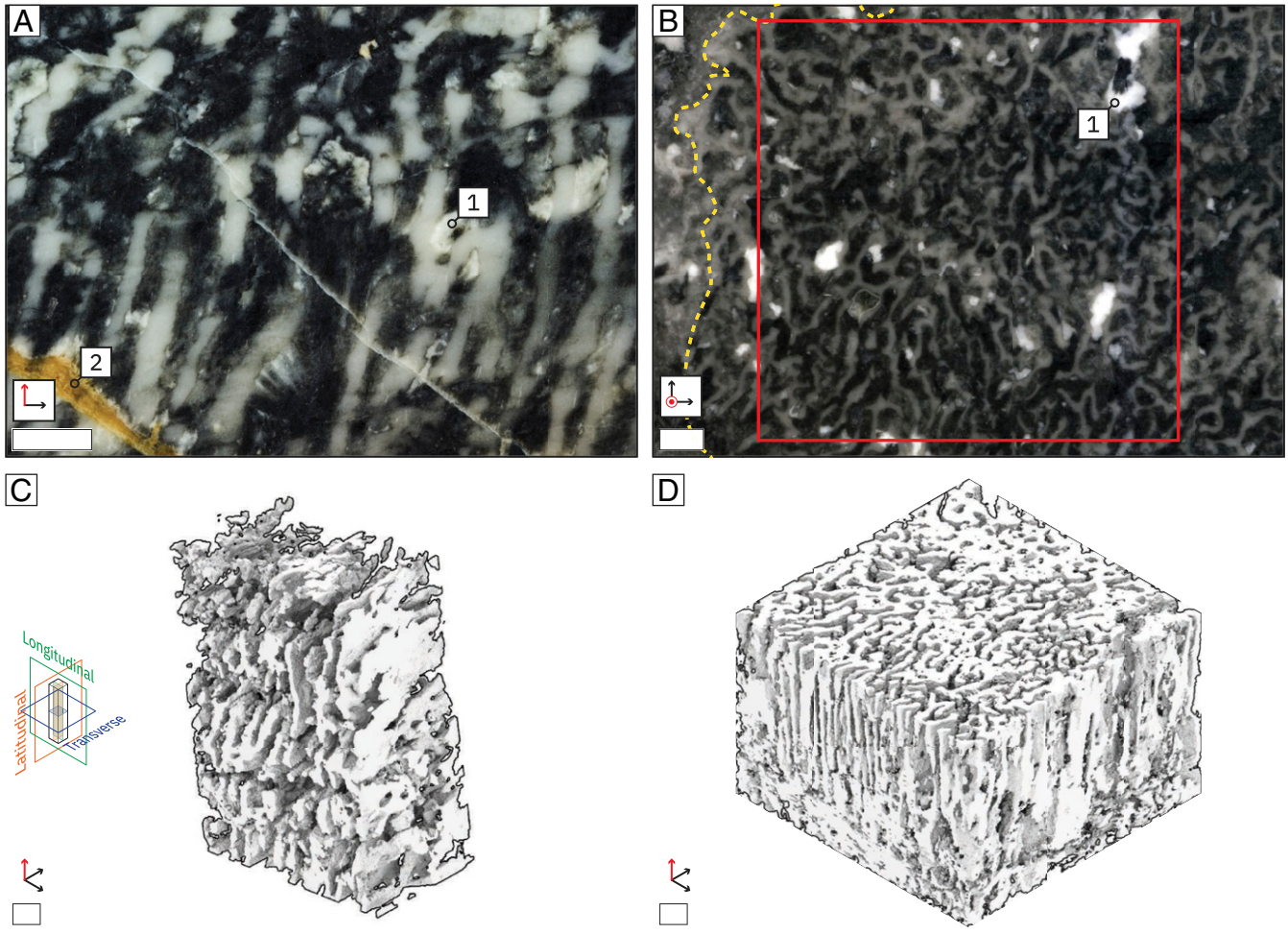

Fig. 2. Reconstructions of *Namapoikia* samples. (*A*) Single slice of *Namapoikia* sample A, processed using GIRI. The circle marker labeled 1 shows blocky calcite that is distributed throughout the sample, while the circle marker labeled 2 is pointing to dolomite filling a fracture within the rock. (*B*) Single slice of *Namapoikia* sample B, processed using a manual serial grinding and imaging procedure (after ref. 6). As the *Namapoikia* specimen is bounded by thrombolite fabrics (denoted using a yellow dotted line), a subregion, marked by the outlined red square, is used for morphological analyses. The circle marker labeled 1 denotes an example of blocky calcite. (*C*) Rendering of the sample A reconstruction. (*Inset*) Diagram illustrating the terms transverse, longitudinal, and latitudinal. (*D*) Rendering of the sample B reconstruction. (Scale bar at the bottom left of each panel, 0.5 cm.) The direction of stratigraphic up is denoted by the red arrow on the axis figure above the scale bar in each panel.

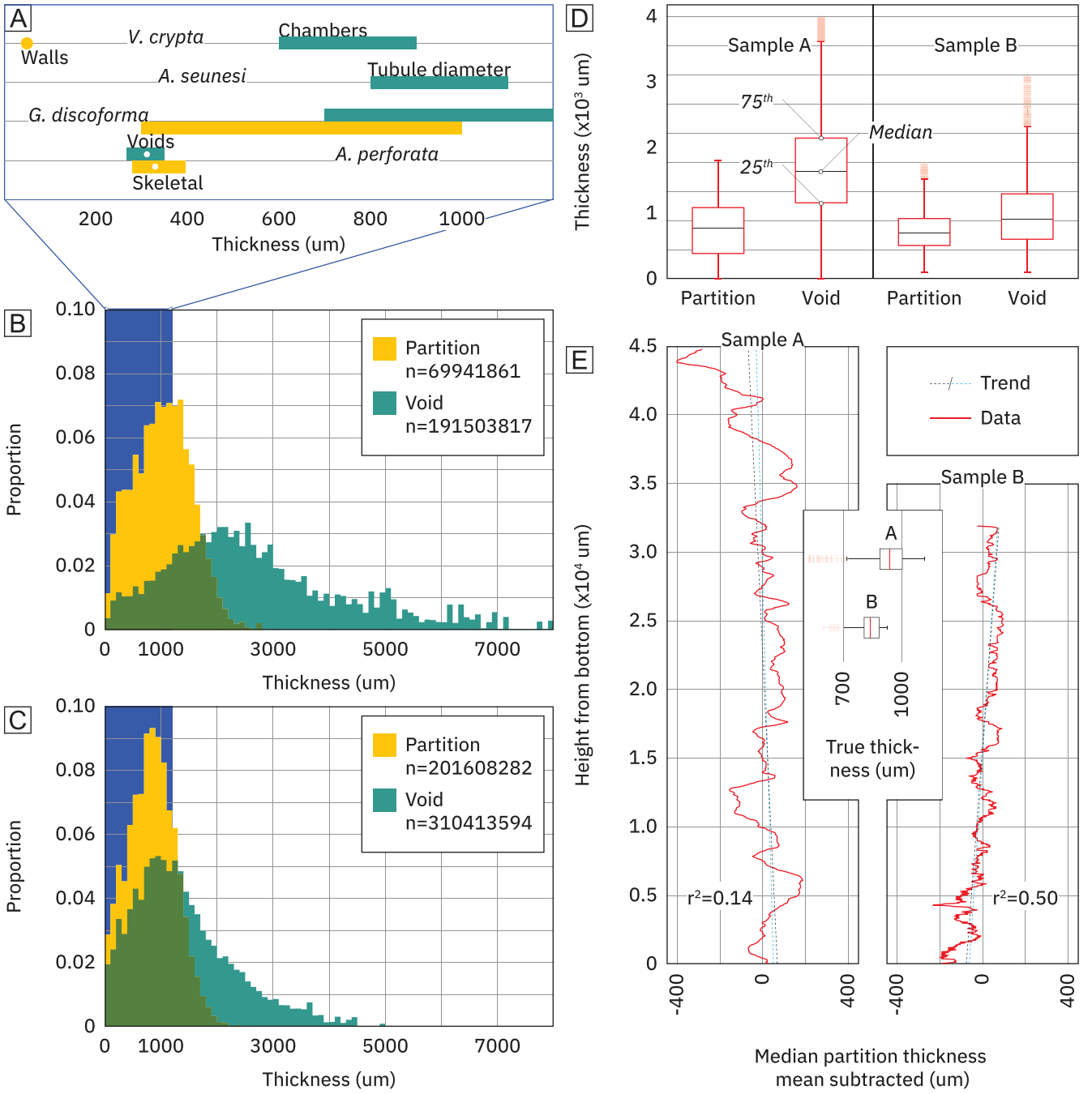

Fig. 3. Measurements made on reconstructions of *Namapoikia* specimens. (*A*) The size of various skeletal elements (and voids) from four different hypercalcified sponges discussed in this study. For *V. crypta*, *A. seunesi*, and *G. discoforma*, bars represent the range of values as reported in literature (refs. 14, 31, and 40, respectively), sometimes from multiple specimens. In the case of *A. perforata* (*SI Appendix*, Fig. S2 *A* and *B*), bars represent the 25th and 75th percentile bounds of measured data from a single specimen, while the white dots depict median values. (*B* and *C*) Histograms illustrating the thickness of partitions and interpartition voids in samples A and B, respectively. The thickness of interpartition voids can be considered equivalent to spacing between partitions. The blue highlighted area depicts the region shown in *A*. (*D*) A comparison of partitions and interpartition void thicknesses from subvolumes selected for their regularly spaced partitions (as described in the text). (*E*) Median partition thickness, mean subtracted, versus height in both samples A and B. Stratigraphic up is in the direction of increasing height, which also is interpreted to be the direction of growth. For each sample, two best-fit trends are shown as dashed lines: in black, the fit takes into account all data, while, in light blue, the fit excludes outliers. Trends are similar even after excluding outliers, so only the r^2 of the dotted black line is denoted. (*Inset*) A box plot showing the range of median partition thicknesses (i.e., as calculated at each sampled height) in both samples.

to the data, the two specimens exhibit different trends, with partitions thinning toward stratigraphic up in sample A and partitions thickening toward stratigraphic up in sample B. In addition to exhibiting low coefficients of determination (Fig. 3*E*), the absolute change of these trends is small relative to a sample's median partition thickness and interpartition spacing. In sample A, the change is 117 μm (or 11% and 6% of median partition and interpartition thicknesses, respectively), while, in sample B, the change is 131 μm (or 16% and 13%).

Discussion

Researchers increasingly believe sponges to be a monophyletic group that—in terms of evolution and phylogeny—should be placed at or near the base of the metazoan tree (24). This group diverged in the Cryogenian, and the last common ancestor (LCA) of modern sponges likely was thin walled, with a single layer of spicules (24) (this prediction is debated, however; see ref. 25 for a counterpoint). From a morphological standpoint, *Namapoikia* is unlike the proposed LCA or even the thin-walled sponges of the early Cambrian [e.g., the Archaeocyathids (18)]. *Namapoikia* does bear a passing resemblance to hypercalcified sponges in the rock record, such as *Vaceletia crypta* and various Inozoa (*SI Appendix*, Figs. S1 and S2). However, 3D reconstructions of *Namapoikia*, with its sheet-like partitions and lack of tabulae or chambers (*SI Appendix*, Fig. S1 *C–F*), make it clear that any apparent morphological similarities are superficial (see *SI Appendix* for a quantitative comparative analysis).

Given the lack of morphological similarities between *Namapoikia* and other described sponges, it may be argued that the fossil represents a stem group poriferan. While exact poriferan synapmorphies are debated, traits unique to *Porifera* include a branching aquiferous system that moves water from pores known as ostia, through choanocyte-bearing chambers, and out one or more osculii (26). Specimens of *Namapoikia* lack any remnants of a clear aquiferous system, ostia, an osculum, and/or any spongin, tissues, or fibers. As a result, a poriferan assignment for *Namapoikia* is doubtful.

An additional challenge to a poriferan affinity for *Namapoikia* comes from the scale of the partitions and voids in observed specimens. While the skeletons of calcareous sponges are not necessarily canal systems, their dimensions are controlled by the scale of living tissue. Both the size and spacing of skeletal elements may be impacted by diagenetic processes (e.g., thickening of calcareous elements at the expense of interpartition void space), the effects of which can be difficult to determine in reconstructions. That said, the combined thickness of partition and interpartition void in *Namapoikia*—a metric which negates the effects of postmortem diagenesis—speaks to a structure that is anomalously large when compared to other poriferans.

Sponges typically produce small-diameter, high-density canal systems to deal with the diffusion processes required for gas exchange and nutrient capture (27). In order to effectively pump water (and overcome resistance/frictional losses), small, densely populated choanocyte chambers are thought to function as peristaltic pumps within sponges (28, 29) (see also ref. 30). Structures built by calcifying sponges generally have features that are submillimeter to a millimeter thick. For example, in the recent hypercalcified demosponge *V. crypta*, which has been proposed to share morphological and biological properties with *Namapoikia* (13), walls and void spaces have a combined thickness of 650 μm to 950 μm (with the walls being 50 μm thick and tissue-bearing chambers ranging from 600 μm to 900 μm in diameter; Fig. 3*A* and ref. 14). *Gigantospongia discoforma*, an exceptionally large hypercalcified sponge (31), has a combined skeletal and canal thickness ranging from 1,000 μm to 2,200 μm (with walls between 300 μm and 1,000 μm thick and tubular canals between 700 μm and 1,200 μm in diameter; Fig. 3*A*).

In our reconstructions, *Namapoikia* partition thicknesses range from 200 μm to 1,650 μm (5th to 95th percentiles for both samples combined), and, even when only examining subvolumes that exclude large voids, *Namapoikia* interpartition thicknesses range from 200 μm to 2,905 μm (5th to 95th percentiles for both samples combined). The combined partition and interpartition thickness of *Namapoikia* (considering all data: 483 μm to 6,425 μm; considering subvolumes only: 300 μm to 4,452 μm) is up to 2.9 times as large as the combined skeletal and canal thickness of *G. discoforma*, one of the largest known sponges.

In addition to producing large and widely spaced structures, *Namapoikia* samples also exhibit significant variance in both partition and interpartition void thicknesses that cannot be explained by selective calcification, even when controlling for irregular voids (Fig. 3 *B–D*). In contrast, sponges (and indeed, all metazoa) produce regularly spaced and sized structures. For example, measurements of voids in *V. Crypta* and *Acanthochaetetes seunesi* (another proposed *Namapoikia* analog), both made on single specimens, show a total range of only 300 μm (~11% of the variation seen in *Namapoikia*; Fig. 3*A*). Taken together, our observations of scale suggest that *Namapoikia* likely created structures too large to be choanocyte bearing (and therefore capable of actively pumping and filter feeding) and too variable to be a regular metazoan construction.

Given our reconstructions, which lack the regularity expected of sponges or, more generally, animals, we suggest that *Namapoikia* was not a metazoan. *Namapoikia*'s morphological expression, which can be summarized as widely spaced, meandering partitions that split and merge both transversely and longitudinally (*SI Appendix*, Fig. S1*F*), likely lacked the structural integrity to stay upright without external support (i.e., much like trying to stand playing cards up on their sides). As a result, *Namapoikia* probably had low emergent synoptic relief (Fig. 4 illustrates this proposed characteristic). We suggest that such a morphological expression can be explained by the growth of partially or totally microbially mediated structures.

Microbially mediated sedimentary constructions, including the stromatolites and thrombolites that make up the reef at Driedoornvlakte Farm, are the result of incremental growth, aggregation, and calcification. The morphologies of such bioconstructions partly are controlled by environmental conditions, including water depth, light levels, and sediment flux (32). In the case of *Namapoikia*, the observed intersample differences in partition and interpartition thicknesses could be explained by variations in local environmental conditions through time and space on the reef. Consistent with our hypothesis is the observation that morphological expressions of microbial constructions often are regional (33). This property would account for why *Namapoikia* is not found cooccurring with *Cloudina* and *Namacalathus* assemblages on other paleocontinents (5, 34, 35).

Both stromatolites—comprising fine laminations—and thrombolites—made up of clotted fabrics—can produce branching forms. Certain thrombolites, such as *Favosamaceria cooperi* (33), also create calcified vertical curtains (referred to as "maceriae" for their likeness to the walls of garden mazes; see *SI Appendix*, Fig. S3 and Movie S4 for our reconstruction). It follows that a microbially mediated construction could produce the morphologies expressed by *Namapoikia*. Fabrics in thrombolites characteristically are millimeter-to-centimeter thick and much less regular in size than metazoans. Thrombolites also contain large, irregularly distributed voids like *Namapoikia* (36). The scale and variance of partitions and interpartition thicknesses, especially within individual *Namapoikia* specimens, are consistent with these attributes of thrombolites.

There is, to the best of our knowledge, no other exactly equivalent microbially mediated structure to reconstruct and compare to *Namapoikia*. Given the influence that environment has on morphological expression of microbial construction, this lack of formal twin is not surprising.

The fractures in which *Namapoikia* is found provided a unique ecological niche in which *Namapoikia* could grow with a distinct morphological expression (Fig. 4). In our model, *Namapoikia* would, at any given moment in time, appear as a series of protruding ridges, which would respond to changing conditions (i.e., light, nutrient, and/or sediment flux) via migration and branching (Fig. 4 *B*, *i–iii*). *Namapoikia* would exhibit low synoptic relief, and the space between partitions would be filled with baffling cement and/or sediment (Fig. 4), so as to provide support to microbial structures that otherwise would deform or topple easily. Thus, the character of longitudinal and transverse branching is indicative of the shape evolution of microbial ridges (Fig. 4*B*) and not the result of coalescing metazoan skeletal walls. Simply put, the final expression of *Namapoikia* represents a collection of multiple, incremental events through time.

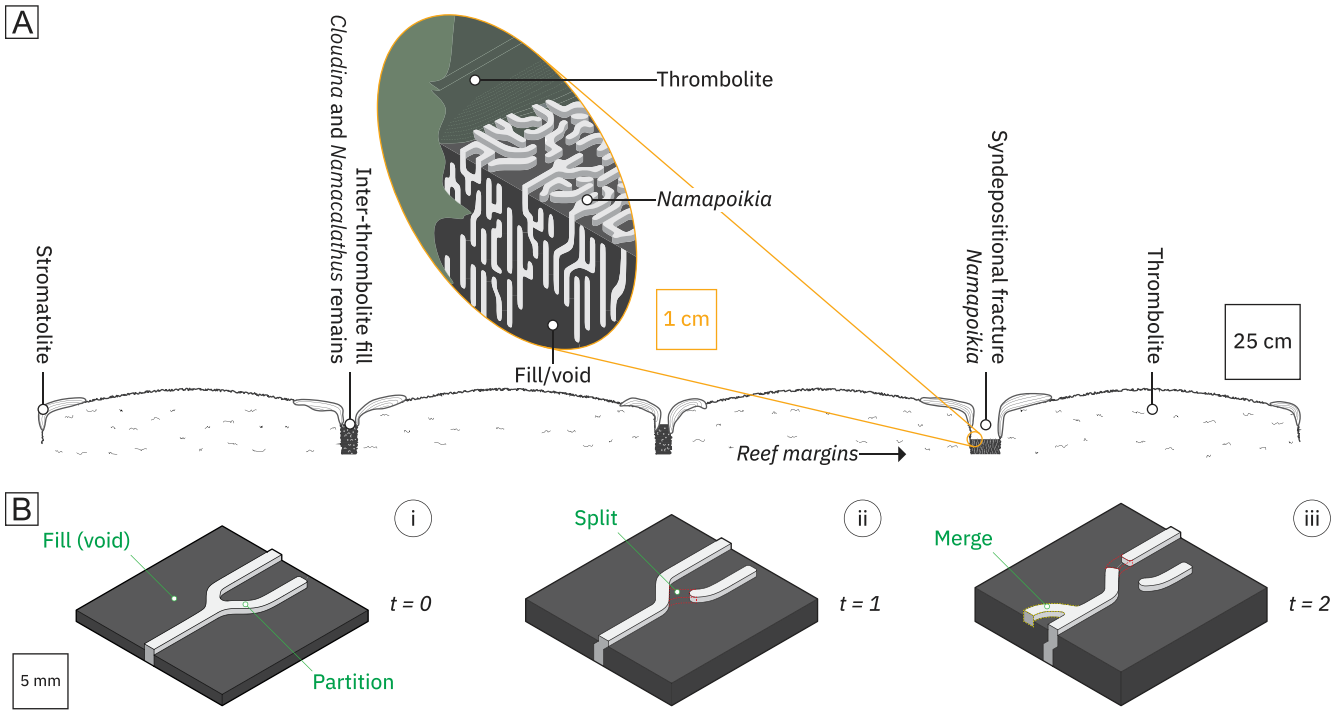

Fig. 4. Diagrams illustrating the proposed model for *Namapoikia*. (*A*) Cartoons depicting the presence of *Namapoikia* in the reef at Driedoornvlakte Farm. *Namapoikia* grew incrementally in syndepostional fissures, interacting with the thrombolites and encrusting stromatolites that made up the reef. (*B*) A model of incremental growth, with only several partitions illustrated. (*i*) Illustration of partitions and void fill at some time 0, with the partitions having low emergent synoptic relief. (*ii*) A second moment in time, where a partition has grown upward and split and migrated. The locations of splits are marked in red. Transverse migrations and meanders of partitions lead to drift in longitudinal cross-section, such that sheet-like partitions may not be perfectly vertical. (*iii*) Partitions have both merged and spilt. The location of the merger is marked in yellow.

Our analyses of *Namapoikia* demonstrate that, in order to assign organismal affinity of problematic fossils based on morphology, 3D observations are required. Quantitative measurements made on reconstructions can both elucidate the presence or absence of structures for use in identification (e.g., testing for tabulae and/or chambers; *SI Appendix*, Fig. S1 *C–F*) and give clues about functional morphology (e.g., the suggestion that *Namapoikia* grew with low synoptic relief). The 3D data provide insights about basic organismal form and function that cannot confidently be extracted using 2D observations alone.

Materials and Methods

Survey Data. To map the spatial extent of various facies, a detailed survey of the pinnacle reef at Driedoornvlakte Farm was conducted. Using a handheld Trimble GeoXH6000 GPS unit (excluding the external antenna), a total of 1,254 GPS points, arrayed on an orthogonal grid with 10 × 20 m spacing, were collected. At each point, a set of discrete keywords—corresponding to visible sedimentological, lithological, and/or physical characteristics—were recorded. The GPS data were differentially corrected using the GPS Pathfinder Office software package at Princeton University. Differential corrections were made with data from the TrigNet Springbok base station, located 654 km from Driedoornvlakte Farm. The corrected data have a mean horizontal accuracy of 0.596 m (SD = 0.126 m) and a mean vertical accuracy of 0.706 m (SD = 0.256 m).

Next, the corrected data—along with associated field observations—were examined for the presence or absence of *Namapoikia*. Points with no evidence of *Namapoikia* were filtered out, and then multiple modeled semivariograms were fit to the resulting empirical (culled) dataset. The best-fit semivariogram (in this case, an exponential with range = 127.69, sill = 0.14, and nugget = 0.10) was used to perform indicator kriging, which resulted in a map of the spatial distributions of *Namapoikia*.

Sample Collection and Serial Grinding. Two *Namapoikia*-bearing samples, referred to as A and B, were collected at Driedoornvlakte Farm for 3D reconstruction. In the case of sample A, the rock's location was recorded with a handheld Trimble GeoXH6000 GPS unit, and its field orientation (i.e., bedding plane direction up) was denoted with arrow markings on multiple faces.

Samples A and B both were slabbed and then mounted on to steel plates using epoxy adhesive. Each sample then was serially sectioned and imaged (final ground dimensions for samples A and B: 41.0 × 57.9 × 19.7 mm and 126.9 × 116.8 × 29.4 mm, respectively).

Sample A was processed using the Grinding, Imaging, and Reconstruction Instrument (GIRI) at Princeton University (11). GIRI comprises a computer numerical control surface grinder that has been retrofitted with misting, wiping, and imaging stages. The imaging stage is made up of an 80-megapixel Phase One IQ180 digital back equipped with a 120-mm Schneider Kreuznach macro lens. This imaging system is positioned vertically so as to attain a 1:1 reproduction ratio at a resolution of 5.73 μm per pixel. For sample A, GIRI programmatically 1) ground away 30 μm of material from the sample surface, 2) wiped off any excess coolant, 3) took an image, 4) evaluated image quality, and 5) then repeated the grinding process a total of 658 times.

Sample B was processed at Massachusetts Institute of Technology (MIT) using a manual serial grinding and imaging procedure. After removing 100 μm of material with a surface grinder, the sample was placed (polished side down) on an EPSON flatbed scanner, and data were recorded at 600 dots per inch resolution (corresponding to a per-pixel resolution of 42.33 μm). This method was repeated 319 times.

For comparative analysis, an *A. perforata* specimen [originally collected by Rigby and Senowbari-Daryan (37)] and an *F. cooperi* specimen were selected for 3D reconstruction. The *A. perforata* sample was processed with GIRI, following the same grinding and imaging procedures as for sample A, with the only difference being a smaller step size (i.e., 20 μm as opposed to 30 μm). A total of 1,624 images of the *A. perforata* specimen were collected, and approximately 1 mm of the sample was preserved and redeposited at the Smithsonian National Museum of Natural History. The *F. cooperi* sample also was processed with GIRI, following the same grinding and imaging procedures as for sample A (with a step size of 30 μm). A total of 391 images of the *F. cooperi* sample were collected.

Image Processing. GIRI outputs data in a proprietary raw image file format (.IIQ), which must be converted to 16-bit RGB TIFF files before further processing. With the exception of applying the same white balance value to all images, the raw data were not adjusted before conversion. Sample B images, which were created as 8-bit JPEG files, required no additional conversion before processing.

Prior to 3D visualization and analysis, images were segmented into distinct classes (e.g., matrix, calcified elements, blocky calcite, and dolomite). Two different neural networks were leveraged for this classification task. In the case of sample A, a hidden layer neural network—operating on superpixels, or pixel clusters made on the basis of color and texture (38)—was used. For sample B, *A. perforata*, and *F. cooperi*, a convolutional neural network was applied.

In all instances, the neural network had to be trained prior to classification. First, a number of representative images—three for sample A, *A. perforata*, and *F. cooperi* and, due to variations in image quality throughout the grinding process, five for sample B—were selected. Next, training data were compiled using a series of custom scripts written in Matlab. For sample A, superpixels were calculated for each image, after which a user selected and assigned superpixels to one of a set of predefined classes via a graphical user interface. Upon completion, a collection of statistics (i.e., the mean, SD, and covariance of Red, Green, and Blue channel values, as well as an entropy term) for each chosen superpixel were calculated and stored in a data structure. In the case of sample B, *A. perforata*, and *F. cooperi*, pixels were painted by a user, thereby marking them as belonging to a given class. For each painted pixel, a square neighborhood (11×11 for sample B and *A. perforata* and 33×33 for *F. cooperi*) was extracted and then stored as a TIFF in a directory corresponding to its assigned class. For both networks, training was accomplished by 1) initializing each neuron within the network with a random weight, 2) running training data through the network to produce a prediction, and 3) updating neuron weights (via stochastic gradient descent with momentum) with the intent of improving network accuracy.

Following training, images of sample A, sample B, *A. perforata*, and *F. cooperi* were run through their respective neural network to produce probability maps, which then were thresholded to create classified TIFFs. These TIFF files then were loaded into Avizo, a software package designed for visualization and analysis of volumetric datasets. In particular, thickness values were generated using the Thickness Map module within Avizo. The module, which implements local thickness as defined by ref. 39, calculates, at each volumetric pixel (or voxel), the diameter of the largest sphere that both is contained in the object (i.e., partition or void) and includes that voxel.

All raw image data are available upon request. The computational source code used to process data in this paper is located in a public repository at https://github.com/giriprinceton/namapoikia.

ACKNOWLEDGMENTS. We thank C. Husselmann for granting us access to Driedoornvlakte Farm. At the Geological Survey of Namibia, G. Schneider and J. Eiseb granted us permits for working in Namibia and assisted us with the export permitting process, respectively. At MIT, B. Ren performed grinding and imaging, and T. Mason created an early reconstruction, of sample B. All of Situ Studio, but especially B. Samuels, were instrumental in the development of GIRI. A. Tasistro Hart and R. Bartolucci provided invaluable assistance in the field. At the Smithsonian, M. Florence dedicated his time to help locate Inozoan specimens for study, while D. Erwin kindly gave permission to destructively analyze the *A. perforata* sample. R. Shapiro generously provided us with a sample of *F. cooperi* for reconstruction. Our morphological analyses benefited from discussions with A. Getraer, B. Howes, R. Manzuk, and E. Geyman. We thank J. Strauss for feedback on the manuscript and A. Knoll and two anonymous reviewers for their thoughtful critique and input. This work was supported by NSF Earth Sciences Grant 1028768 to A. Maloof and by funding from the Princeton Tuttle Invertebrate Fund.

1. Ulf. Linnemann *et al.*, New high-resolution age data from the Ediacaran–Cambrian boundary indicate rapid, ecologically driven onset of the Cambrian explosion. *Terra. Nova* **31**, 49–58 (2019).
2. S. M. Rowland, R. A. Gangloff, Structure and paleoecology of lower Cambrian reefs. *Palaios* **3**, 111–135 (1988).
3. Y. Cai, S. Xiao, G. Li, H. Hong, Diverse biomineralizing animals in the terminal Ediacaran Period herald the Cambrian explosion. *Geology* **47**, 380–384 (2019).
4. A. Y. Zhuravlev, R. A. Wood, A. M. Penny, Ediacaran skeletal metazoan interpreted as a lophophorate. *Proc. Biol. Sci.* **282**, 20151860 (1818).
5. J. P. Grotzinger, W. A. Watters, A. H. Knoll, Calcified metazoans in thrombolite-stromatolite reefs of the terminal Proterozoic Nama Group, Namibia. *Paleobiology* **26**, 334–359 (2000).
6. W. A. Watters, J. P. Grotzinger, Digital reconstruction of calcified early metazoans, terminal Proterozoic Nama Group, Namibia. *Paleobiology* **27**, 159–171 (2001).
7. S. W. Grant, Shell structure and distribution of Cloudina, a potential index fossil for the terminal Proterozoic. *Am. J. Sci.* **290**, 261–294 (1989).
8. P. U. P. A. Gilbert *et al.*, Biomineralization by particle attachment in early animals. *Proc. Natl. Acad. Sci. U.S.A.* **116**, 17659–17665 (2019).
9. A. M. Penny *et al.*, Ediacaran metazoan reefs from the Nama Group, Namibia. *Science* **344**, 1504–1506 (2014).
10. A. Shore, R. Wood, A. Curtis, F. Bowyer, Multiple branching and attachment structures in cloudinomorphs, Nama Group, Namibia. *Geology*, 10.1130/G47447.1 (2020).
11. A. Mehra, A. C. Maloof, Multiscale approach reveals that *Cloudina* aggregates are detritus and not in situ reef constructions. *Proc. Natl. Acad. Sci. U.S.A.* **115**, E2519–E2527 (2018).
12. Z. Chen, S. Bengtson, C. M. Zhou, H. Hong, Y. Zhao, Tube structure and original composition of Sinotubulites: Shelly fossils from the late neoproterozoic in southern Shaanxi, China. *Lethaia* **41**, 37–45 (2008).
13. R. Wood, A. Penny, Substrate growth dynamics and biomineralization of an Ediacaran encrusting poriferan. *Proc. Biol. Sci.* **285**, 20171938 (2018).
14. J. Vacelet, "Recent "Sphinctozoa", order Verticillitida, family Verticillitidae Steinmann, 1882" in *Systema Porifera*, J. N. A. Hooper, R. W. M. Van Soest, Eds. (Springer, 2002), pp. 1097–1098.
15. E. A. Sperling, J. M. Robinson, D. Pisani, K. J. Peterson, Where's the glass? Biomarkers, molecular clocks, and microRNAs suggest a 200-myr missing Precambrian fossil record of siliceous sponge spicules. *Geobiology* **8**, 24–36 (2010).
16. J. B. Antcliffe, R. H. T. Callow, M. D. Brasier, Giving the early fossil record of sponges a squeeze. *Biol. Rev.* **89**, 972–1004 (2014).
17. B. J. Nettersheim *et al.*, Putative sponge biomarkers in unicellular Rhizaria question an early rise of animals. *Nature Ecol. Evol.* **3**, 577–581 (2019).
18. J. P. Botting, B. J. Nettersheim, Searching for sponge origins. *Nature Ecol. Evol.* **2**, 1685–1686 (2018).
19. A. C. Maloof *et al.*, Possible animal-body fossils in pre-Marinoan limestones from South Australia. *Nat. Geosci.* **3**, 653–659 (2010).
20. J. Grotzinger, E. W. Adams, S. Schröder, Microbial–metazoan reefs of the terminal proterozoic Nama Group (c. 550–543 Ma), Namibia. *Geol. Mag.* **142**, 499–517 (2005).
21. E. W. Adams, S. Schröder, J. P. Grotzinger, D. S. McCormick, Digital reconstruction and stratigraphic evolution of a microbial-dominated, isolated carbonate platform (terminal Proterozoic, Nama Group, Namibia). *J. Sediment. Res.* **74**, 479–497 (2004).
22. J. P. Grotzinger, S. A. Bowring, B. Z. Saylor, A. J. Kaufman, Biostratigraphic and geochronologic constraints on early animal evolution. *Science***270**, 598–604 (1995).
23. R. A. Wood, J. P. Grotzinger, J. A. D. Dickson, Proterozoic modular biomineralized metazoan from the Nama Group, Namibia. *Science* **296**, 2383–2386 (2002).
24. J. P. Botting, L. A. Muir, Early sponge evolution: A review and phylogenetic framework. *Palaeoworld* **27**, 1–29 (2018).
25. C. Luo, F. Zhao, Z. Han, The first report of a vauxiid sponge from the Cambrian Chengjiang Biota. *J. Paleontol.* **94**, 28–33 (2020).
26. C. W. Dunn, S. P. Leys, S. H. D. Haddock, The hidden biology of sponges and ctenophores. *Trends Ecol. Evol.* **30**, 282–291 (2015).
27. J. U. Hammel *et al.*, The non-hierarchical, non-uniformly branching topology of a leuconoid sponge aquiferous system revealed by 3D reconstruction and morphometrics using corrosion casting and X-ray microtomography. *Acta Zool.* **93**, 160–170 (2012).
28. P. S. Larsen, H. U. Riisgård, The sponge pump. *J. Theor. Biol.* **168**, 53–63 (1994).
29. H. U. Riisgård, P. S. Larsen, Comparative ecophysiology of active zoobenthic filter feeding, essence of current knowledge. *J. Sea Res.* **44**, 169–193 (2000).
30. S. P. Leys *et al.*, The sponge pump: The role of current induced flow in the design of the sponge body plan. *PloS One* **6**, e27787 (2011).
31. J. Keith Rigby, B. Senowbari-Daryan, *Gigantospongia*, new genus, the largest known Permian sponge, Capitan limestone, Guadalupe Mountains, New Mexico. *J. Paleontol.* **70**, 347–355 (1996).
32. T. Bosak, A. H. Knoll, A. P. Petroff, The meaning of stromatolites. *Annu. Rev. Earth Planet Sci.* **41**, 21–44 (2013).
33. R. S. Shapiro, S. M. Awramik, *Favosamaceria cooperi* new group and form: A widely dispersed, time-restricted thrombolite. *J. Paleontol.* **80**, 411–422 (2006).
34. H. J. Hofmann, E. W. Mountjoy, Namacalathus-Cloudina assemblage in Neoproterozoic Miette Group (Byng Formation), British Columbia: Canada's oldest shelly fossils. *Geology* **29**, 1091–1094 (2001).
35. J. E. Amthor *et al.*, Extinction of Cloudina and Namacalathus at the Precambrian-Cambrian boundary in Oman. *Geology* **31**, 431–434 (2003).
36. L. C. Kah, J. P. Grotzinger, Early Proterozoic (1.9 Ga) thrombolites of the Rocknest Formation, Northwest Territories, Canada. *Palaios* **7**, 305–315 (1992).
37. J. Keith Rigby, B. Senowbari-Daryan, *Upper Permian Inozoid, Demospongid, and Hexactinellid Sponges from Djebel Tebaga Tunisia* (University of Kansas, 1995).
38. R. Achanta *et al.*, SLIC superpixels compared to state-of-the-art superpixel methods. *IEEE Trans. Pattern Anal. Mach. Intell.* **34**, 2274–2282 (2012).
39. T. Hildebrand, P. Rüegsegger, A new method for the model-independent assessment of thickness in three-dimensional images. *J. Microsc.* **185**, 67–75 (1997).
40. K. Rützler, J. Vacelet, "Family Acanthochaetetidae Fischer, 1970" in *Systema Porifera*, J. N. A. Hooper, R. W. M. Van Soest, Eds. (Springer, 2002), pp. 275–278.